Terr. Atmos. Ocean. Sci., Vol. 32, No. 1, 113-131, February 2021 doi: 10.3319/TAO.2020.10.15.01

Impacts of falling ice radiative effects on projections of Southern Ocean sea ice change under global warming

Jui-Lin F. Li[1, *], Wei-Liang Lee[2], Kuan-Man Xu[3], Jonathan Jiang[1], Eric Fetzer[1], Chao-An Chen[2], Pei-Chun Hsu[2], Huang-Hsiung Hsu[2], Jia-Yuh Yu[4], and Yi-Hui Wang[5]

[1] *Jet Propulsion Laboratory, California Institute of Technology, Pasadena, CA, USA*
[2] *RCEC, Academia Sinica, Taipei City, Taiwan*
[3] *Science Directorate, NASA Langley Research Center, Hampton, VA, USA*
[4] *Department of Atmospheric Sciences, National Central University, Taoyuan City, Taiwan*
[5] *California Polytechnic State University, San Luis Obispo, CA, USA*

Article history:

Received 16 May 2020
Revised 12 October 2020
Accepted 15 October 2020

Keywords:

Southern Oceans, Sea ice, Falling ice, GCM, Climate changes, Radiation

Citation:

Li, J.-L. F., W.-L. Lee, K.-M. Xu, J. Jiang, E. Fetzer, C.-A. Chen, P.-C. Hsu, H.-H. Hsu, J.-Y. Yu, and Y.-H. Wang, 2021: Impacts of falling ice radiative effects on projections of Southern Ocean sea ice change under global warming. Terr. Atmos. Ocean. Sci., 32, 113-131, doi: 10.3319/TAO.2020.10.15.01

ABSTRACT

The falling ice (snow) radiative effects (FIREs) have previously been shown to contribute substantially to reduced discrepancies in simulations of present-day climatology of radiation, skin temperatures and sea ice concentration and thickness over the Southern Ocean. This study extends to examine the impacts of FIREs on simulation of sea ice changes under a scenario of gradual increase of atmospheric CO_2 concentration. We perform a pair of sensitivity experiments including (CESM1-SoN) and excluding (CESM1-NoS) FIREs using Community Earth System Model version 1. The differences in the annual and seasonal means between the initial and warmer periods are examined. Relative to CESM1-SoN, CESM1-NoS simulates more surface reflected shortwave and less downward longwave radiative warming, as well as colder surface temperature, resulting in larger annual-mean sea ice extent and thickness and slower seasonal and long-term sea ice melting and thinning. Over the Southern Ocean of CESM1-SoN, reduced downwelling longwave radiation in austral winter (June-July-August: JJA) leads to sea-ice growth with colder skin temperature while reduced net radiation resulting from increased shortwave reflection in austral summer reduces the melting of sea ice with little change in skin temperature. CESM1-NoS shows seasonal and long-term trends similar to those in CMIP5 models that exclude FIREs, hinting slower future warming-driven changes and larger amplitude of the annual cycle in sea ice concentration and thickness. The ice-free Southern Ocean in peak melting season is simulated at approximately year 130 for CESM1-NoS but year 100 for CESM1-SoN, about 30 years later than that of the Arctic.

1. INTRODUCTION

Southern Ocean sea ice change is critically important for Earth's global energy balance and atmosphere-ocean heat transport (Lefebvre and Goosse 2007; Stammerjohn et al. 2008; Maksym et al. 2012; Meijers et al. 2012; Intergovernmental Panel on Climate Change: IPCC 2013; Mahlstein et al. 2013; Meijers 2014). Forty years of satellite observations showed a gradual, decades-long overall increase in Antarctic sea ice extents reversed in 2014, with subsequent rates of decrease in 2014 - 2017 far exceeding the more widely publicized deceasing rates experienced in the Arctic (Parkinson 2019). Extents for 2017 and 2018 were the lowest on record for both austral winter maximum and summer minimum. In 2019, both the minimum and maximum extents fell below the 1981 - 2010 average, but neither was a record low for that time of year (Scott 2019). Understanding the processes behind these changes is vital to improve estimates of albedo feedbacks, i.e., the change in Earth's net heat absorption from reflection changes in response to temperature change. In contrast to the small observed sea ice increases before 2014, most coupled global climate models (CGCMs) simulate decreased Antarctic sea ice extent over

* *Corresponding author*
E-mail: jli@jpl.nasa.gov

the past 30 years (e.g., Maksym et al. 2012; Li et al. 2017).

Processes contributing to the sea ice change, in particular the earlier growth, include stronger cyclonic flow over West Antarctica, dynamical changes in Southern Annular Mode (SAM, Turner and Overland 2009) and strengthening of the cold, southerly winds blowing northward from the Ross Ice Shelf, which could increase vertical mixing and cooling of waters off the continental shelf (Comiso 2009). Although the observed Ross Sea sector extent increased, it decreased in the Bellingshausen-Amundsen sector (Comiso et al. 2011). Sea ice near West Antarctica was also found to be influenced by the Amundsen Sea Low (ASL, Raphael et al. 2016), which is being driven by ocean circulation changes. Therefore, the aforementioned evidence for large internal variability limits our ability to extract the forced response from observations.

Several recent studies used simulations from the Community Earth System Model Large Ensemble (CESM-LE) to argue that the modeled Southern Oceans sea ice changes in the Coupled Model Intercomparison Project Phase 5 (CMIP5) model ensemble might be influenced by internal climate variability and the CMIP5 ensemble members are due to inter-model realizations of internal variability alone (Turner et al. 2013, 2015; Zunz et al. 2013; Kay et al. 2015; Armour et al. 2016; Rosenblum and Eisenman 2017). For example, the observed and modeled Antarctic sea ice expansion is the result of internal climate variability surpassing modeled sea ice retreat that would have occurred due to climate forcing suggesting the role of simulated internal variability to explain the differences between typical state-of-the-art climate model simulations and observed sea ice trends in Southern Oceans (Polvani and Smith 2013; Turner et al. 2013). There is a paradox of the influence from the above-mentioned internal variability that was not reproduced by the CESM-LE (Kay et al. 2015; Rosenblum and Eisenman 2017), suggesting other factors might be important to consider such as global mean temperature trend for sea ice expansion over Southern Oceans (Rosenblum and Eisenman 2017). These studies suggest that the consensus on the influences of the internal variability on climate simulations is still far from reached.

Many present-day CGCMs, including those in CMIP5, exhibit large spreads with nontrivial biases in Southern Ocean sea ice extent (Taylor et al. 2012; Li et al. 2017), with some simulating less than one-third of the observed annual mean extent (Bracegirdle et al. 2008, 2015; Turner et al. 2013) and much larger seasonal changes (Van den Broeke 2004; Simmonds 2015; Li et al. 2017), suggesting that sea-ice melting rates are unrealistically high in some CGCMs. Thus, there is low confidence in Antarctic sea ice projections (Turner and Overland 2009; Maksym et al. 2012; Turner et al. 2013; Zunz et al. 2013; Smith et al. 2014; Hosking et al. 2016; Li et al. 2017).

Reported IPCC CMIP5 simulations project decreased sea ice extent between 1986 - 2005 and 2081 - 2100, with a mean decrease of 16 - 67 % in February (minimum sea ice area) and 8 - 30 % in September (maximum sea ice area), depending on the amount of global warming in the designated scenarios (IPCC 2013). About 75% of CMIP5 models reach a nearly ice-free state in February before 2100 under the most extreme forcing scenario, the Representative Concentration Pathway 8.5 (RCP8.5). Only small portions of the Weddell and Ross Seas stay ice-covered in February during 2081 - 2100.

The Antarctic and Southern Ocean climate systems are the result of complex interactions between external forcing, large-scale nonlinear climate dynamics and regional feedbacks. Given the wide spread of CMIP5 simulations and the importance of the Southern Ocean for climate feedbacks (Armour et al. 2013), it is important to assess the physical processes that can bias model projections. Identifying these bias sources and reducing them should contribute to reduce uncertainties in climate change projections. A physical understanding of the link from simulated historical sea ice changes to projected changes is also important because an accurate representation of observed sea ice extent is a necessary condition for producing realistic projections (Bracegirdle et al. 2015; Li et al. 2017).

A number of physical processes have been shown to contribute to differences in CGCM representations of the energy budget and sea ice in the Southern Ocean, including the abundance and brightness of clouds (Trenberth and Fasullo 2010), the lack of supercooled liquid clouds (Cesana et al. 2012; McCoy et al. 2015; Kay et al. 2016a, b), and the importance of regional topography and bathymetry (Nghiem et al. 2016). The representation of the cloud effects can impact local radiation and thus contribute to sea ice changes (Kay et al. 2016a), but it is a challenge for CGCMs to have the correct radiative representation of cloud and precipitating hydrometeors such as falling ice (snow). Because the atmospheric moisture-holding capacity will increase in a warming climate, falling ice (snow) is expected to grow into the future (Medley et al. 2018), which may increase the radiative effect of snow that further impacts the sea ice extent and thickness.

In majority of CMIP5 models, falling ice (snow) radiative effects (FIREs) are excluded, and in this study, we attempt to quantify the impact of FIREs to simulated Antarctic sea ice changes under global warming. An earlier study has shown that inclusion of FIRE reduces model-observation discrepancy of the present-day Southern Ocean sea-ice concentration (Li et al. 2017). That study used controlled simulations with a climate model in which FIRE was enabled or not. With FIREs, the longwave radiation warming restricted wintertime sea ice growth, resulting in a lower summertime albedo, and lower sea ice extent continued throughout the

ice melting season compared with a simulation that excluded FIREs. The inclusion of FIREs resulted in a reduced sea ice extent bias relative to observations by (0.17×10^6 km^2, 39%) in summer and (2.12×10^6 km^2, 55%) in winter (JJA). In this study, this FIRE mechanism and its importance to the Antarctic and Southern Ocean sea ice projection will be extensively examined in the context of progressive global warming, in particular, assessing how FIRE may affect projected temperature and sea ice changes over the Southern Ocean, compared to the Arctic sea ice projection presented in Li et al. (2020). They found that both surface temperature and net radiation changes are equally important to sea ice change in the Arctic.

The model sensitivity experiments and analysis methods are described in section 2. In section 3, the potential impact of FIRE on sea ice change is examined. Results are discussed and major findings are presented in section 4.

2. METHODS

2.1 Climate Model Simulations

To isolate the impacts of FIRE, we perform a pair of fully-coupled simulations, as in Li et al. (2017, 2020): one includes precipitating-ice (snow) radiative effects (CESM1-SoN or SoN) and the other excludes snow radiative effects (CESM1-NoS or NoS). The Community Earth System Model version 1 (CESM1) is used, which is managed by National Center for Atmospheric Research (NCAR) and Department of Energy (DOE). CESM1 is composed of five separate model components that simultaneously simulate the Earth's atmosphere, ocean, land surface, land ice, and sea-ice. Model code and documentation are available from http://www.cesm.ucar.edu/models/cesm1.0/.

The atmospheric component is the Community Atmosphere Model version 5 (CAM5). The model uses a two-moment stratiform cloud microphysics scheme which allows snow mass flux at each model level and time step to be diagnosed. Snow represents falling large crystals and its radiative effect is included in the radiation code using the diagnosed mass and effective radius of snow crystals (Morrison and Gettelman 2008; Gettelman et al. 2010; Neale et al. 2012). Simulated present-day ice and snow mass was comparable to that in CloudSat-CALIPSO retrieved products (Gettelman et al. 2010).

Both climate change simulations are initialized from their respective achieved hundreds of years of preindustrial control (piControl) runs by following the CMIP5 1pctCO2 protocol, in which atmospheric CO_2 increases at 1% yr^{-1} for 140 years. This results in an ultimate quadrupling of CO_2 by the end of the simulations. In this study, we choose years 1 - 20 inclusive as the control period and years 121 - 140 as the comparison period, with differences mimicking those that would occur in a future warmer climate.

2.2 Analysis Method

The surface energy balance and its connection with the surface skin surface temperatures (Ts) and other parameters, including sea ice concentration (SIC), is analyzed following the methodology of earlier studies (Li et al. 2017, 2020; Lee et al. 2019).

The magnitudes of the area-averaged (over 50 - 70°S ocean only; including sea ice coverage) surface downward shortwave flux ($SW_\downarrow$), surface downward longwave flux ($LW_\downarrow$), and surface upward shortwave flux ($SW_\uparrow$) are much larger than latent heat flux (LHF: ~10 - 20 W m^{-2}) and sensible heat flux (SHF: ~2 - 15 W m^{-2}). Sea ice restricts surface turbulent energy, moisture and momentum exchange, which can affect precipitation, ocean waves and circulation (Aagaard 1989; Aagaard and Carmack 1989; Beszczynska-Möller et al. 2011; Bintanja and Selten 2014; Palerme et al. 2017). Assuming negligible contributions from LHF and SHF compared to net radiation contributions (~100 - 250 W m^{-2}) and a small net heat uptake or release from the surface, the surface energy budget may be written:

$$\epsilon\sigma T_s^4 \cong SW_\downarrow + LW_\downarrow - SW_\uparrow \quad (1)$$

where ϵ is the surface emissivity, σ the Stefan-Boltzmann constant, T_s the surface skin temperature, and SW and LW refer to shortwave and longwave fluxes, respectively, with arrows denoting their direction. The combination of the three radiative fluxes on the right-hand-side of Eq. (1) is for the response of surface thermal emission, that is $LW_\uparrow = \epsilon\sigma T_s^4$, which can be called "approximated net input flux for surface-emitting longwave radiative flux" (referred as AELW). For short, it is called "net radiative flux (Net)" with respect to the net surface radiative flux and the response to the atmospheric radiative flux input. In other words, Net flux implicitly includes the small contributions from SHF and LHF.

We use the two 1pctCO2 simulations with CESM1-CAM5 described in section 2.1: CESM1-SoN (snow radiative effect on) and CESM1-NoS (snow radiative effect off). In addition, twelve CMIP5 models with 1pctCO2 simulations are considered (Table 1), and the ensemble mean (CMIP5-NoS) or the Multi-Model Mean (MMM) of 11 models (i.e., excluding CESM1) is compared with CESM1-SoN and CESM1-NoS simulations since none of the CMIP5 models includes FIREs except for CESM1.

We found that the results are insensitive to averaging periods of 10 - 30 years length, and we present 20-year averages here. Figure 1 introduces the notation that describes each comparison. We examine the differences between CESM1-NoS and CESM1-SoN, hereafter, NoS-SoN or denoted as $\delta(\ )$. We use CESM1-SoN as a reference in the comparisons presented in this study since Li et al. (2017)

showed that present-day radiative flux and sea ice biases are reduced when including FIREs. By doing this, $\delta(\ )$ represents the opposite sign of the impact of FIREs. We then examine the climate change component by subtracting the mean years 1 - 20 from that of years 121 - 140, and denoted this as $(\ )'$. The difference in simulated climate change related to FIREs is the difference between CESM1-NoS and CESM1-SoN for the change between two climates, which is donated as $\delta(\ )'$.

As in Li et al. (2017), we average over 50 - 70°S to include the majority of the sea ice but minimize differences due to inconsistent land-sea masking among models. For both CESM1-SoN and CESM1-NoS and CMIP5-NoS simulations, we examine the surface radiative energy budget components: upward and downward longwave and shortwave fluxes, as well as surface skin surface temperature and sea ice thickness (THK) and sea ice concentration (SIC).

3. RESULTS

3.1 Impacts of FIRE on the Long-Term Trend and the Seasonal Cycle

Figures 2a and b show time series of annual-mean SIC and sea ice area for CESM1-NoS, CESM1-SoN and CMIP5-NoS averaged over the 50 - 70°S latitude belt for the entire simulation period (140 years). The long-term sea-ice melting rate (or trend) in the CMIP5-NoS (-0.065% per year or -0.0278 million km^2 per year) is slower than CESM1-NoS (-0.104% per year or -0.044 million km^2 per year), but they match with each other extremely well for the last 80 years. Both have slower SIC melting rates relative to CESM1-SoN (-0.116% per year or -0.049 million km^2 per year). The fact that CMIP5-NoS has a slower rate than either CESM1-NoS or CESM1-SoN may suggest that other physical processes in CMIP5 models are likely involved besides the inclusion of FIRE, especially in the first 50 years, when CMIP5-NoS and CESM1-NoS differ more than between CMIP5-NoS and CESM1-SoN. It is interesting that the trend is overlapped to each other after year 50 between CMIP5-NoS and CESM1-NoS.

The time series of sea ice can behave differently among seasons because both sea ice thickness and area are affected by the annual cycle of solar radiation and associated changes in the atmospheric and oceanic dynamics. We examine the different impacts of FIREs on the ocean-only area averages of SIC, thickness and snowfall on sea ice area (SNOW) over the belts 50 - 70°S of CESM1-SoN and CESM1-NoS simulations for March-April-May: MAM, June-July-August: JJA, September-October-November: SON, and December-January-February: DJF seasons (Fig. 3). As in the annual mean time series (Fig. 2), SIC (Figs. 3a - d) and thickness (Figs. 3e - h) are higher in CESM1-NoS than in CESM1-SoN for all four seasons, but their differences are much larger during the sea ice forming season in JJA than during the other three seasons MAM, SON, and DJF. During the melting season (MAM), CESM1-SoN shows a faster sea ice melting rate than CESM1-NoS. That is, sea ice in CESM1-SoN nearly disappears (~1%) approximately in year 100 while in year 130 for CESM1-NoS. Similar to SIC, sea ice thickness (THK; Figs. 3e - h) is thicker (20 - 50 cm) in CESM1-NoS than in CESM1-SoN with similar long-term trends that nearly approaching to zero depth for MAM. However, snowfall on sea ice area (SNOW; Figs. 3i - l) has the opposite differences, with more SNOW in CESM1-SoN suggesting the contribution from snowfall on the sea ice surface is very small (~0.1 cm) and cannot be a factor for contributing to more SIC/THK in CESM1-NoS. This result suggests that there is little impact in the mass balance for sea ice simulation.

It is apparent that the divergence at year 60 shown in Fig. 2 between CESM1-NoS and CESM1-SoN for both SIC and THK is most pronounced during the sea ice forming season (JJA, Figs. 3b and f) with an accelerated change in THK for the later part of the simulation. This accelerated change is also seen in other three seasons but they are slightly weaker than in JJA. This result is caused by the surface warming due to FIREs (as explained later), which reduces the sea ice thickness more rapidly over the remaining sea ice area as SIC decreases with time.

We further compare seasonal cycle of SIC for CESM1-NoS and CESM1-SoN against CMIP5 model groups. Figures 4a - c show the seasonal cycles of each of 12-member CMIP5 group (gray lines) and the ensemble mean (blue line), along with the multi-model-mean (MMM) plus/minus one standard deviation (green lines) averaged over 50 - 70°S for the first, middle (years 61 - 80), and last 20 years. Figures 4d - f show the seasonal cycles of CESM1-SoN (red) and CESM1-NoS (black) simulations over the same region and periods. The amplitudes of SIC are all reduced from first, middle to last under progressive warming. Both CESM1-NoS and CESM1-SoN lie within the CMIP5 distribution and close to MMM for all three periods. In general, the CMIP5-NoS MMM mean annual cycle is similar to CESM1-NoS, with minimum in February/March and maximum in September, but with higher SIC during the peak period (June - November). Both CMIP5-NoS MMM and CESM1-NoS simulate higher SICs than CESM1-SoN throughout most of the annual cycle, in particular, for the middle and last periods as climate warms and sea ice melts. The amplitude of SIC annual cycle in CESM1-SoN is, thus, greatly reduced, compared to CESM1-NoS and individual CMIP5-NoS models.

3.2 Impacts of FIRE on 140-Year Climatology

Figures 5 and 6 show the significant levels ($p < 0.05$) for the seasonal-mean difference between CESM1-NoS and CESM1-SoN in radiation fields, Ts and SIC and THK

Table 1. A list of 12 coupled atmosphere-ocean climate models in CMIP5 archive under 1%CO2 (1pctCO2) used in this study.

Model	Description
ACCESS1-3	Commonwealth Scientific and Industrial Research Organisation, and Bureau of Meteorology (Australia)
BCC-CSM1-1	Beijing Climate Center, China Meteorological Administration (China)
BCC-CSM1-1-m	Beijing Climate Center, China Meteorological Administration (China)
BNU-ESM	College of Global Change and Earth System Science, Beijing Normal University (China)
CanESM2	Canadian Centre for Climate Modelling and Analysis (Canada)
CCSM4	National Center for Atmospheric Research (USA)
CNRM-CM5	Centre National de Recherches Meteorologiques / Centre Europeen de Recherche et Formation Avancees en Calcul Scientifique (France)
IPSL-CM5A-LR	Institut Pierre-Simon Laplace (France)
MIROC-ESM	Japan Agency for Marine-Earth Science and Technology, Atmosphere and Ocean Research Institute (The University of Tokyo), and National Institute for Environmental Studies (Japan)
MPI-ESM-LR	Max Planck Institute for Meteorology (MPI-M) (Germany)
MRI-CGCM3	Meteorological Research Institute (Japan)
NorESM1-ME	Norwegian Climate Centre (Norway)

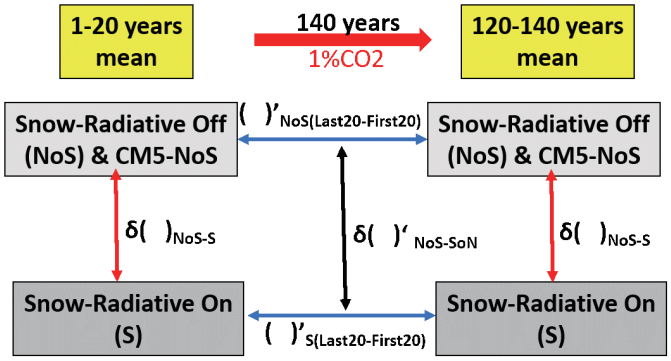

Fig. 1. A schematic diagram describing the sensitivity experiment and analysis method in this study. δ( ) represents the differences between Snow-radiative effects off (NoS) and Snow-radiative effects On (S or SoN) for both initial climate from the first 20 years and future climate from the last 20 years. ( )' represents the changes by subtracting the annual mean of the first 20 years from that of the last 20 years in both SoN and S (SoN) cases. δ( )' is calculated from the differences in the changes of ( )' between SoN and S (SoN) cases. The same analysis is applied for CMIP5 (see Table 1) 1pctCO2 from eleven CGCMs without snow-radiative effects (CM5-NoS).

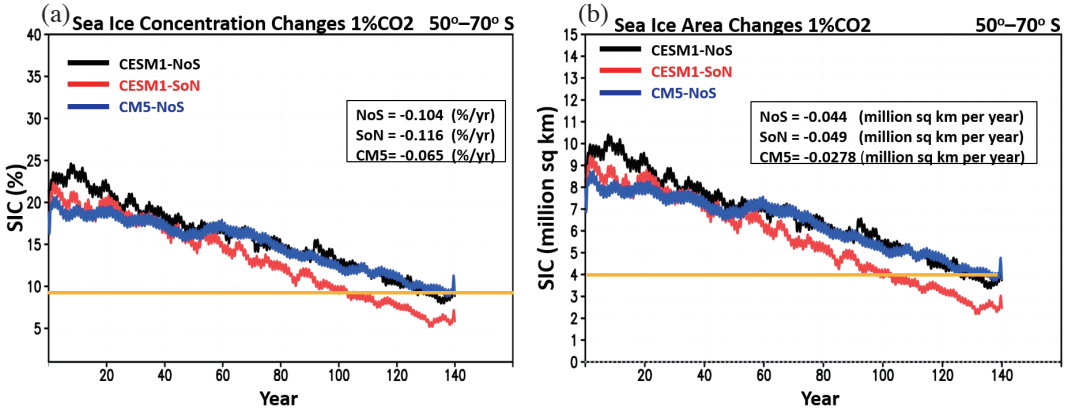

Fig. 2. (a) Time series of annual-mean sea ice concentration (%) for CESM1 snow-radiative effects off (CESM1-NoS: black line), CESM1 snow-radiative effects on (CESM1-SoN: red line) and CMIP5 multi-model mean (CMIP5-MMM or CM5-NoS: blue line) averaged over the latitude belts 50 - 70°S under 1%CO2 per year (1pctCO2) for 140 years. (b) Same as (a) but for sea ice area. The yellow lines are added for reference to illustrate the corresponding year of CESM1-SoN and CESM1-NoS and CM5-NoS when a certain SIC value is reached.

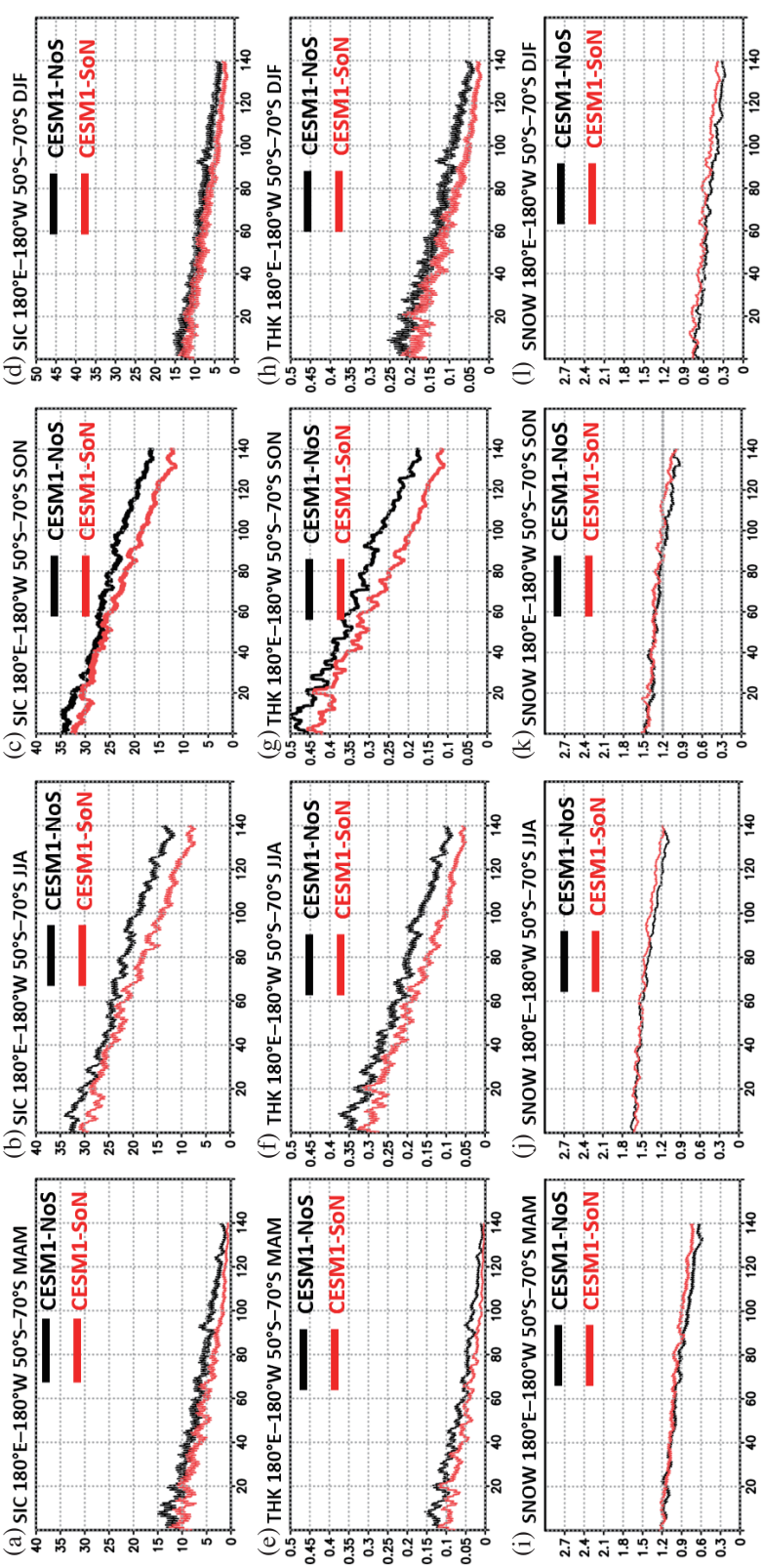

Fig. 3. Time series of sea ice concentration (%) for CESM1 snow-radiative effects off (CESM1-NoS: black line) and CESM1 snow-radiative effects on (CESM1-SoN: red line) averaged over the latitude belt of 50 - 70°S under 1%CO2 per year (1pctCO2) for 140 years for (a) March-April-May (MAM), (b) June-July-August (JJA), (c) September-October-November (SON), and (d) December-January-February (DJF). (e) - (h) Same as (a) - (d) but for sea ice thickness (THK: meter) while (i) - (l) same as (a) - (d) but for snow on sea ice area (SNOW: m), respectively.

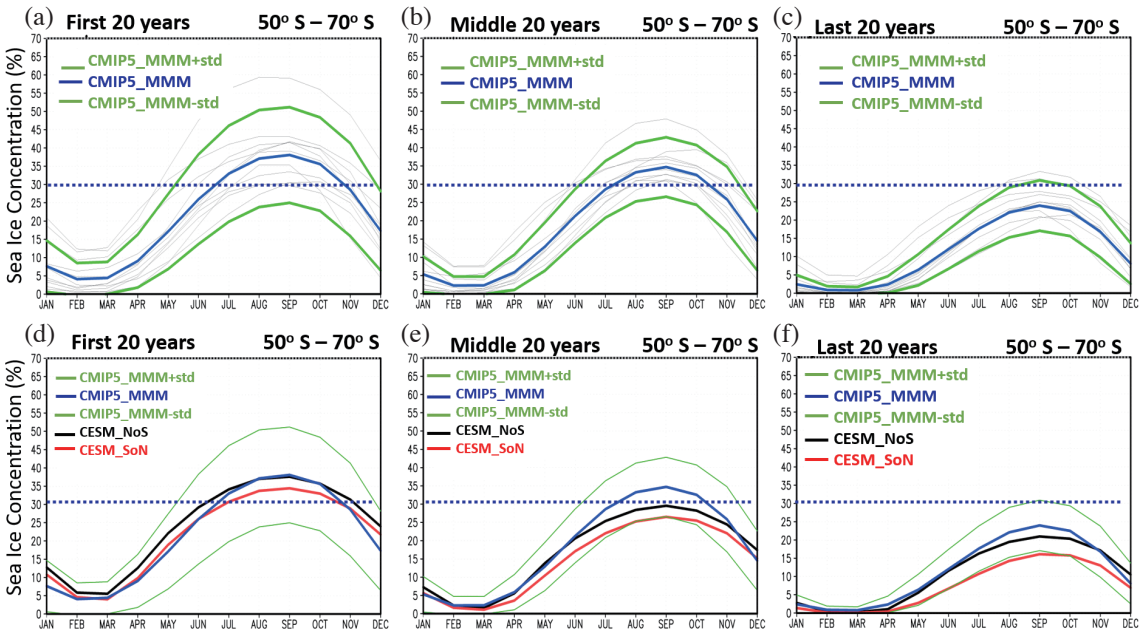

Fig. 4. Mean seasonal cycle of sea-ice concentration (SIC) of each CMIP5 model (thin black lines), the multi-model mean (MMM: blue line), and one standard deviation (green lines) averaged over 50 - 70°S for (a) the first (years 1 - 20), (b) middle (years 61 - 80), and (c) last 20 (years 121 - 140) years. (d) - (f) is the same as (a) - (c) but for the MMM seasonal cycle (blue line) with one standard deviation (green lines), and the seasonal cycle of snow-radiative effects off (CESM1-NoS: black), and snow-radiative effects on (CESM1-SoN: red), respectively. Dotted lines at 30% are used for comparison among the first, middle and last stages.

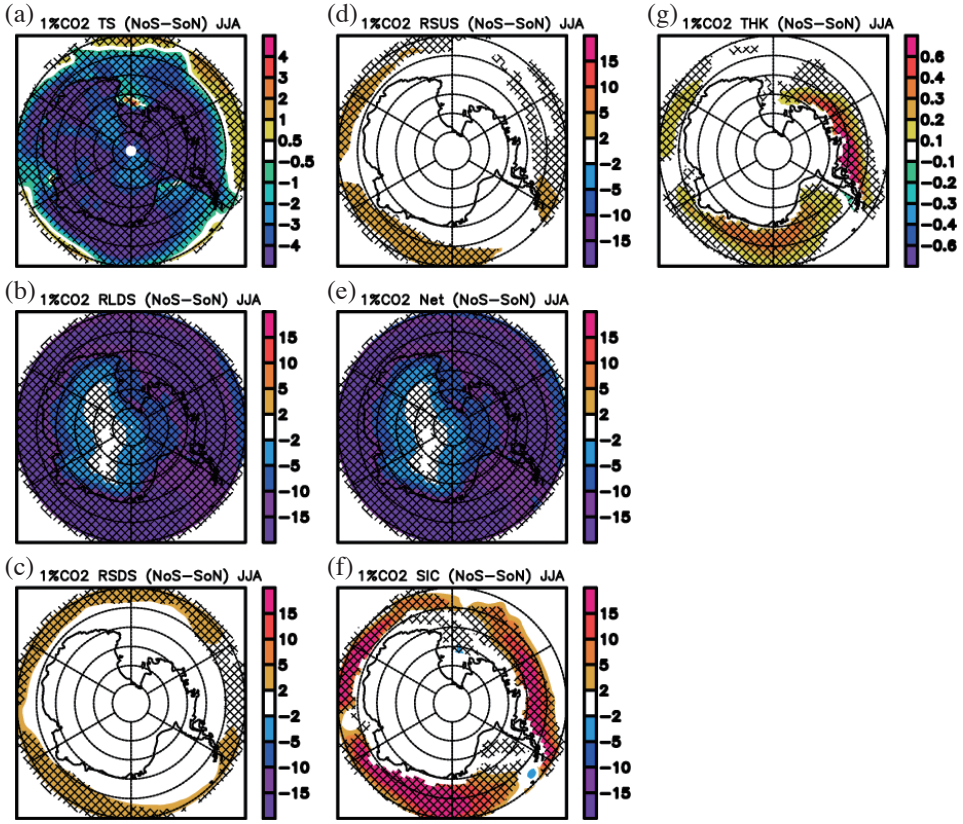

Fig. 5. Difference between CESM1 falling ice radiative effects (FIRE) off minus on (NoS-SoN) for June-July-August (JJA) mean for 140 years in 1pctCO2 scenario for (a) skin temperature (TS: K), (b) downward surface longwave radiation (RLDS: W m^{-2}), (c) downward surface shortwave radiation (RSDS: W m^{-2}), (d) upward surface shortwave radiation (RSUS: W m^{-2}), (e) sea ice concentration (SIC: %), and (f) sea ice thickness (THK: cm). The shaded area represents the significant levels ($p < 0.05$).

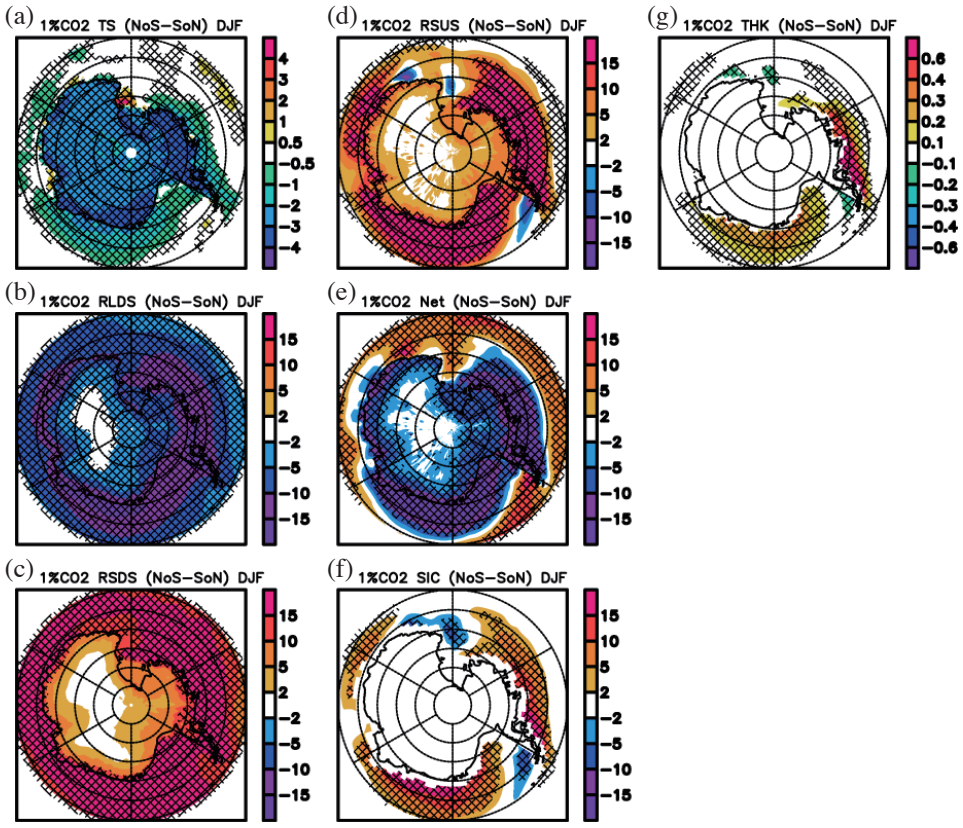

Fig. 6. Same as Fig. 5 but for December-January-February (DJF).

for austral winter, JJA (Fig. 5), and austral summer, DJF (Fig. 6), averaged over the 140 years. The stippled areas over the plots indicate that the NoS-SoN differences are all significant for RLDS and Net in JJA (Fig. 5) and RSDS, RSUS, and Net in DJF (Fig. 6) over the entire study domain except for a small part of Antarctic continent, leading to the significant changes in skin temperature, SIC and sea ice thickness over the Southern Ocean sea ice-covered regions (also over the continent for Ts).

For the differences in 140-year averaged surface radiative fluxes, Ts, SIC, and THK between CESM1-NoS and CESM1-SoN, CESM1-NoS produces colder Ts (Figs. 5a, 6a), which lead to increases in SIC (Figs. 5f, 6f) and sea ice thickness (Figs. 5g, 6g) relative to CESM1-SoN. The colder Ts, located towards higher latitudes in austral summer (Fig. 6a) than in austral winter (Fig. 5a), is due to less AELW, i.e., Net (heating) (Figs. 5e, 6e), up to 15 W m^{-2} that is contributed mainly from reducing surface downward longwave (up to and 15 W m^{-2}) (RLDS) (Figs. 5b, 6b), and increasing summer (DJF) surface downward shortwave flux RSDS (Fig. 6c) and their counteracting (cooling) upward shortwave fluxes (up to 15 W m^{-2}) (Fig. 6d). The AELW differences are highly correlated with less RLDS, colder Ts and more SIC (up to 15%) and THK (up to and 0.6 m) in winter while more RSDS, RSUS and SIC/THK in summer for CESM1-NoS than CESM1-SoN. These results are consistent with Li et al. (2017) but for the climatology under progressive warming.

3.3 Impacts of FIREs on Changes of Annual-Mean Climatology from Years 1 - 20 to 121 - 140

As discussed in Li et al. (2017) for the present-day climate simulations, total ice-water path is underestimated by about 100 g m^{-2} (~80% relative to total ice water path) over much of the Southern Ocean, contributing to an underestimate in downward longwave radiation ($LW_{\downarrow}$) and an overestimate in downward shortwave radiation at the surface ($SW_{\downarrow}$) and overestimate in reflected shortwave (indirectly from increasing sea ice albedo). This falling ice radiative effect leads to a reduction of the model-observed discrepancy in sea-ice area. The improvement in sea-ice area simulation with FIREs is driven by an increase in downward longwave radiation ($LW_{\downarrow}$), which restricts the growth of sea ice during sea-ice forming season, and by decreased reflection of sunlight at surface during sea-ice melting season, which might be due to the delayed effect from the reduced sea ice from the previous winter (details referred to Li et al. 2017).

Figures 7a - c show the impacts of FIREs on the initial 20-year mean state of annual-mean SIC, AELW, and

Ts simulations. Relative to the CESM1-SoN simulation, the CESM1-NoS simulation generates high spatial coherence of more SIC (peak magnitude > 15%) and less AELW (< -15 W m^{-2}) that are associated with colder Ts (from -2 to -3 K) over two regions, i.e., Region 1: 180 - 40°W, 60 - 68°S (Southern Ocean starting from dateline eastward to Weddell Sea) and Region 2: 60 - 160°W, 60 - 65°S (Bellingshausen Sea and Amundsen Sea). The largest changes in Region 1 occurs near the 60°S latitude circle while parts of Region 1 (70°E - 180) experience slightly smaller values of colder Ts (-1 to -2K). Figures 7d - f show the same differences in the spatial patterns but with stronger impacts for the last 20-year mean state. That is, except that there is a pattern shift to higher latitudes around 90 - 150°W and to eastward in 30°E - 30°W, it is evident that the spatial patterns of SIC, AELW, and Ts maintain the similar differences in a progressive warmer climate with the magnitudes of the differences being amplified, compared to the initial 20-year mean state. These larger differences are indicated by much colder Ts (by < -3 K, Fig. 7f), less AELW (< -15 W m^{-2}), and more SIC forming (> 15%) over the same region, compared to CESM1-SoN. It is also interesting to note that SIC is changed from reduction to increase in parts of Weddell Sea between the two climates. The differences in SIC near the 60°S latitude circle between CESM1-NoS and CESM1-SoN are smaller, especially, in Region 2 (between 65°S and 70°S), due to ice-free states. However, the opposite occurs between 20°E and 20°W. These results reflect the differences in regional sea ice melting (Fig. A6c for changes in sea ice thickness) as climate warms.

Given the high spatial coherence between patterns of aforementioned differences in surface radiative fluxes, Ts and SIC for both the initial and warmer climate states, we will next examine the impact of FIREs on progressive warming by quantifying the contributions from each surface radiative component and the impacts to Ts and SIC. Figure 8 shows the differences between the last and first 20-year periods and between CESM1-NoS and CESM1-SoN simulations, that is, the climate of last 20-year of (NoS-SoN) minus first 20-year annual mean climate of (NoS-SoN) (see Fig. 1), Over the two regions discussed earlier, in particular, near the Weddell Sea to Kong Hakon VII Sea and Bellingshausen Sea to Amundsen Sea, we find a causal link and progressive changes from the initial toward warmest climates as follows: models excluding FIRE produce colder Ts (Fig. 8a), due to less AELW (Fig. 8b) that is contributed from reducing surface downward longwave (Fig. 8c), and increasing reflected surface shortwave flux (Fig. 8d) and downward shortwave fluxes (Fig. 8e), and increasing SIC (Fig. 8f). The changes in these radiative components contribute to changes in AELW (Net), driving changes in sea-ice concentration (Fig. 8g) and sea ice thickness in the late period (Figs. A6a - c). The sensitivity of decreasing SIC rate per unit AELW can be up to -0.2 ~ -0.3 (%/W m^{-2}) with small regional variations although there are large regional variations for Ts, AELW, and SIC. This causal link between SIC and radiative fluxes discussed above is also dependent on the seasonal cycle. During dark Antarctic winters (JJA) the LW warming effects dominate, which contributes to AELW, and during a short period in summer (DJF), the SW cooling effects dominate resulting in small net SW over sea ice due to the high surface albedo.

3.4 Impacts of FIRE on Changes of Seasonal Surface Energy Budget and Sea-Ice Concentration

Since the contributions from SW fluxes are negligibly small during austral winter but the largest in austral summer, it is important to further qualify the impact of seasonal changes of FIRE on progressive warmer climates and highlight the relationships of SIC with SW and LW radiative fluxes. We will discuss the results for austral winter, June-July-August (JJA) and austral summer, December-January-February (DJF) of CESM1 simulations. Figure 9 shows the progressive climate changes of the model NoS-SoN maps of (Figs. 9a, g) skin temperatures (Ts), (Figs. 9b - e, h - k) radiation budget components, and (Figs. 9f, l) sea-ice concentration for summer in DJF and winter in JJA.

3.4.1 Austral Summer (DJF)

Under a warmer climate relative to initial climate state in austral summer (Figs. 9a - f), CESM1-NoS produces slightly colder Ts (up to -1 to -2 K) with larger decreasing net flux (-15 W m^{-2}) than the CESM1-SoN simulation along with more sea ice concentration (~15%) over sea ice regions, especially over the western hemisphere of the two regions mentioned earlier and mostly poleward of 70°S. Except for the poleward shift of zero change locations, these features are largely similar to those in the annual mean presented in Fig. 8. CESM1-NoS produces more SIC than CESM1-SoN near Weddell Sea (Fig. 9f), resulting in more SIC in the annual mean shown in Fig. 8f and thicker sea ice (Fig. A6d), which is related to stronger surface reflected SW (Fig. 8d). The larger amount of sea ice over the higher latitudes (Fig. 9f) reflects more solar radiation than the downward solar radiation, which contributes greatly to the net surface cooling there in summer (Fig. 9b).

Over the lower (< 70°S) latitudes of Amundsen Sea (Fig. 9f), summertime sea ice melting seen in other locations is nonexistent due to thicker sea ice there (Fig. A6d). This is associated with little change in Ts but with more change in AELW (Net cooling), which is associated with larger changes in decreased reflected SW than downward SW.

The abovementioned results indicate that, during austral summer (DJF), the relationship between radiative flux and SIC changes is complex. In some regions, such as off the coast of Dronning-Maud land, there is a net increased

change in downward shortwave radiation ($SW_{\downarrow}$ - $SW_{\uparrow}$) with increased sea-ice reflected SW along with a net increase in sea-ice concentration (figure not shown). This seasonal change indicates the little increased summer longwave heating but with more downward and reflected SW, helping sea-ice growth over higher latitudes and leading to a higher surface albedo there. This increased reflected SW is sufficiently large to offset the reduction in downward shortwave radiation and longwave heating at the surface, helping summertime sea-ice growth in these regions. On the other hand, melting over lower latitudes accelerates as reflected SW increases without FIREs.

3.4.2 Austral Winter (JJA)

For austral winter (JJA) when solar radiation contributes little to the net flux (AELW) changes, the changes in the net flux (Fig. 9h) with magnitude up to -15 W m^{-2} are dominated by less downward LW radiation changes (Fig. 9i), leading to broader regions with colder Ts (up to -2 to -3 K) than the SoN simulation along with more sea ice concentration (~15%) over sea ice regions. That is, without FIREs included (CESM1-NoS), the sea ice formation accelerates in austral winter, instead of decelerates, over the higher latitudes of Southern Oceans in a progressive warmer climate relate to CESM1-SoN. Over parts of the lower latitudes, however, there are large areas of warmer Ts change, increasing net flux and decreasing SIC, compared to the annual mean. This result suggests a stronger role of Ts in sea ice melting as climate warms, compared to austral summer in NoS than SoN as the meridional temperature gradient increases.

It is important to point out the seasonal contributions from each radiation component (Summer: Figs. 9c - e and Winter: Figs. 9i - k) to SIC changes. These figures illustrate that the SoN simulation produces consistently lower surface radiative fluxes but higher sea ice concentration in a progressive warming climate over sea ice regions (60 - 70°S; referred to as lower latitudes earlier) than the NoS simulation. The dominant part of FIREs is the reduced downward longwave flux, up to -15 W m^{-2} in JJA (Fig. 9i). Compared to that in JJA, the dominant part of FIREs in DJF is the shortwave reflection over the same region (Fig. 9d), from approximately +15 W m^{-2}. Of the above changes, we see reduced model representation of downwelling longwave radiation in austral winter (JJA) that restricts austral winter sea-ice growth with colder Ts. In austral summer (DJF), due to less net radiation increases (Fig. 9b), the melting of sea ice is substantially reduced, relative to the NoS simulation.

The lack of FIREs in the CESM1-NoS simulation also increases the sea ice melting in austral spring and sea ice forming in austral fall (see Fig. A2). Also shown in Fig. A3, the changes of surface snowfall from last 20-year and first 20-year are increased both in CESM1-NoS (Fig. A3a) and CESM1-SoN (Fig. A3b) in DJF as well as in JJA (Figs. A3d, A3e), due to the fact that the atmospheric moisture holding capacity will increase in a warmer climate. However, the NoS-SoN differences in surface snowfall under progressive warming do not show many changes as shown in Fig. A3c for DJF and Fig. A3f for JJA except for a

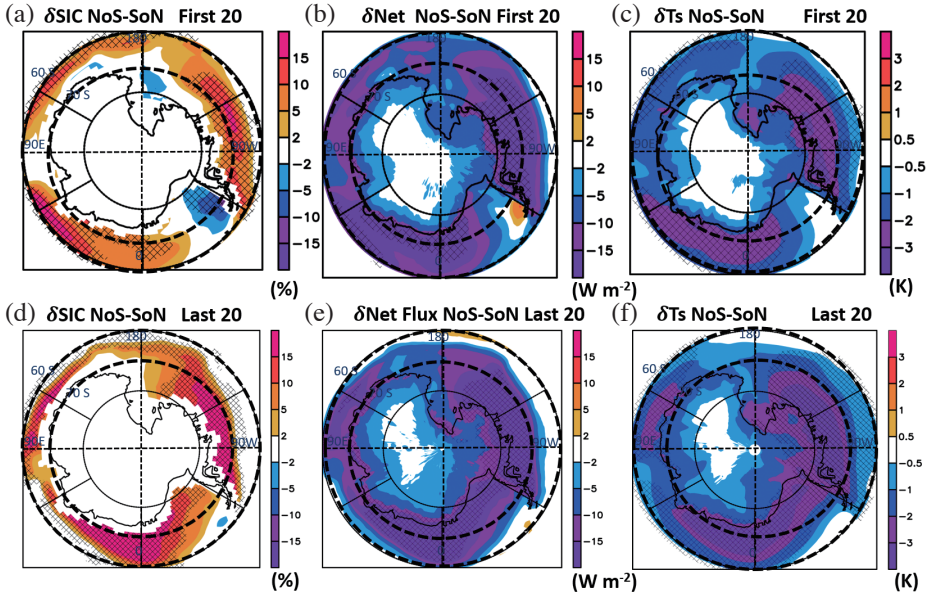

Fig. 7. The difference between Snow-Radiative off minus Snow-radiative on (NoS-SoN) annual mean from the first 20 years (1 - 20 years) for (a) sea ice concentration, δSIC (%); (b) surface net flux, δNet (W m^{-2}); and (c) surface skin temperature δTs, (K). (d) - (f) Same as (a) - (c) but for the annual mean from the last 20 years (120 - 140 years). The SoN and SoN are CESM1 experiments integrated for 140 years, following the CMIP5 1pctCO2 scenario. The shaded area represents the significant levels ($p < 0.05$).

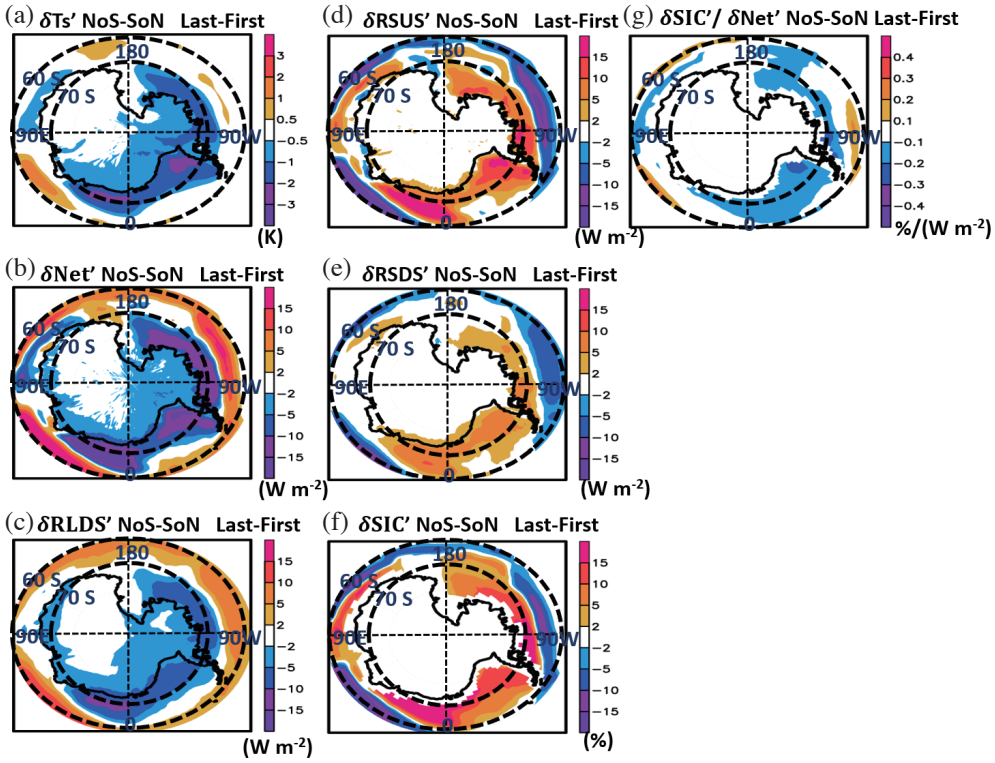

Fig. 8. As in Fig. 7, but for the changes between last 20 years and first 20 years in 1pctCO2 scenario (i.e., the last 20 years minus the first 20 years) from SoN minus SoN for (a) surface skin temperature, δTs'; (b) surface net flux, δNet'; (c) surface downward longwave radiation, δRLDS'; (d) surface upward shortwave radiation, δRSUS'; (e) surface downward shortwave radiation, δRSDS'; (f) sea ice concentration, δSIC'; and (g) the ratio of absolute change of SIC to that of Net, δSIC'/δNet', from NoS-SoN.

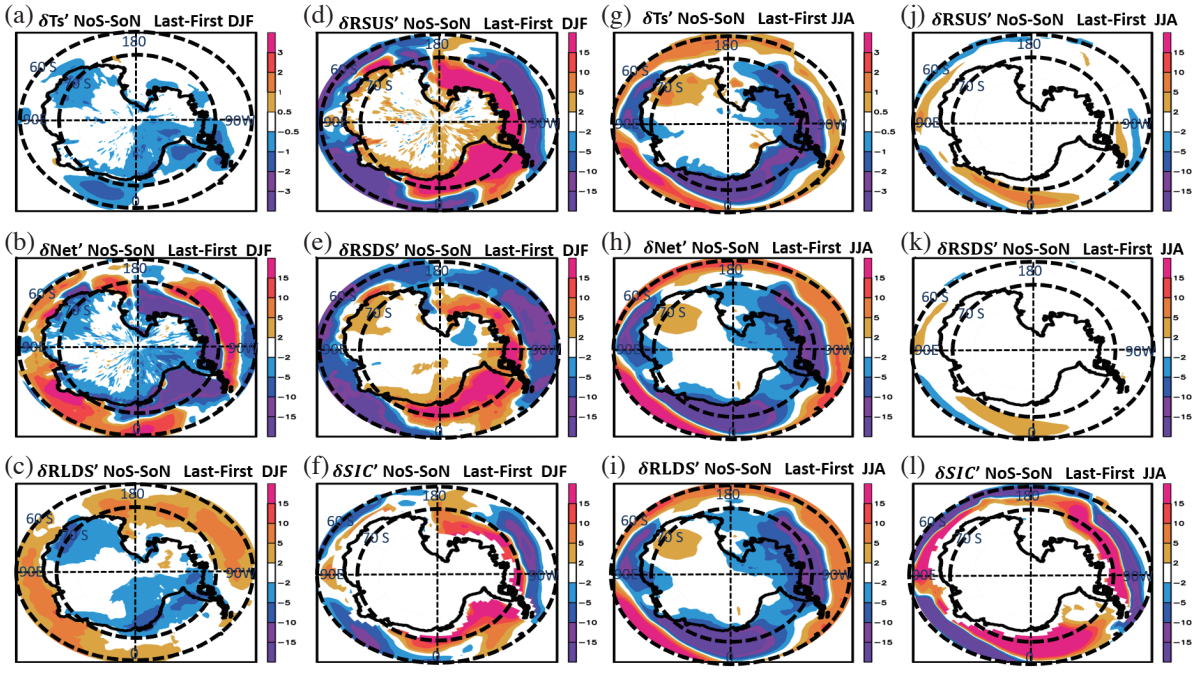

Fig. 9. As in Fig. 8, but for December-January-February (DJF) for (a) surface skin temperature, δTs'; (b) net flux, δNet'; (c) surface downward longwave radiation, δRLDS'; (d) surface upward shortwave radiation, δRSUS'; (e) surface downward shortwave radiation, δRSDS'; and (f) sea ice concentration, δSIC', from NoS-SoN. (g) - (l) Same as (a) - (f) but for June-July-August (JJA).

few small areas. This implies that there is no significant contribution of mass adding from snowfall to the SIC changes between CESM1-NoS and CESM1-SoN.

3.5 Comparisons with CMIP5 Models

It is difficult to justify the confidence level is reliable for projection of how the sea ice will evolve under global warming for a CGCM. The fact that CESM1-CAM5 with FIREs outperforms the case without FIREs in present-day constrained by observations reported in Li et al. (2017) allows us to use CESM1-SoN as a reference to compare our climate projection results in the context of multi-model mean as in previous studies (e.g., Bracegirdle et al. 2015; Li et al. 2017). We choose CESM1-SoN as a reference for comparisons against CMIP5 MMM (CMIP5-NoS) in a progressive warmer climate.

The results are shown in Fig. 10 (Ts, SIC, and Net flux) and Appendix Fig. A1 (radiative budget components) for the changes in the annual-mean climatology between the last and first 20 years periods. The aforementioned tendency changes in terms of patterns from CESM1-NoS relative to CESM1-SoN (Figs. 10a - c) are very similar to the CMIP5 MMM against CESM1-SoN (i.e., CMIP5-NoS minus SoN) (Figs. 10d - f) in the differences but with broader covered regions than NoS minus SoN of CESM1. The changes of RLDS, RSDS, RSUS, and net flux between CESM1-SoN and CMIP5 are non-trivial with magnitudes larger than at least 10 - 15 W m^{-2} in latitude belts in 70°S—coast of Antarctic continent but with opposite changes between the latitude belts in 60 - 70°S. The annual mean changes of each of four radiative flux components (surface downward SW, LW, and SW reflection to surface net flux; Fig. A1) are generally similar between CESM1-NoS minus CESM1-SoN and CMIP5-NoS minus SoN except with larger magnitudes and broader covered regions with the same signs of changes. Also, the seasonal changes in CMIP5 multi-model ensemble against CESM1-SoN (i.e., CMIP5NoS-SoN) (Fig. A4 for DJF and Fig. A5 for JJA) are similar to the differences between CESM1-NoS and CESM1-SoN except with broader covered regions. The above broader regions seem to be the product of ensemble average resulted from large model spread in simulating the regional characteristics of progressive climate changes among CMIP5 models. Differences in model physical processes other than FIREs may contribute to model spread.

4. DISCUSSION AND CONCLUSIONS

FIREs have been found to be one of the important contributions in reducing present-day mean-state biases in terms of radiation, skin temperatures, and sea ice extent of the Southern Ocean both in CESM1 and CMIP5-MMM (e.g., Li et al. 2017). Li et al. (2017) found that with the inclusion of FIREs, the surface radiation budgets and skin temperature and sea ice content improved dramatically against observations in present-day simulation. FIREs contribute substantially to alleviate the discrepancy that commonly exists

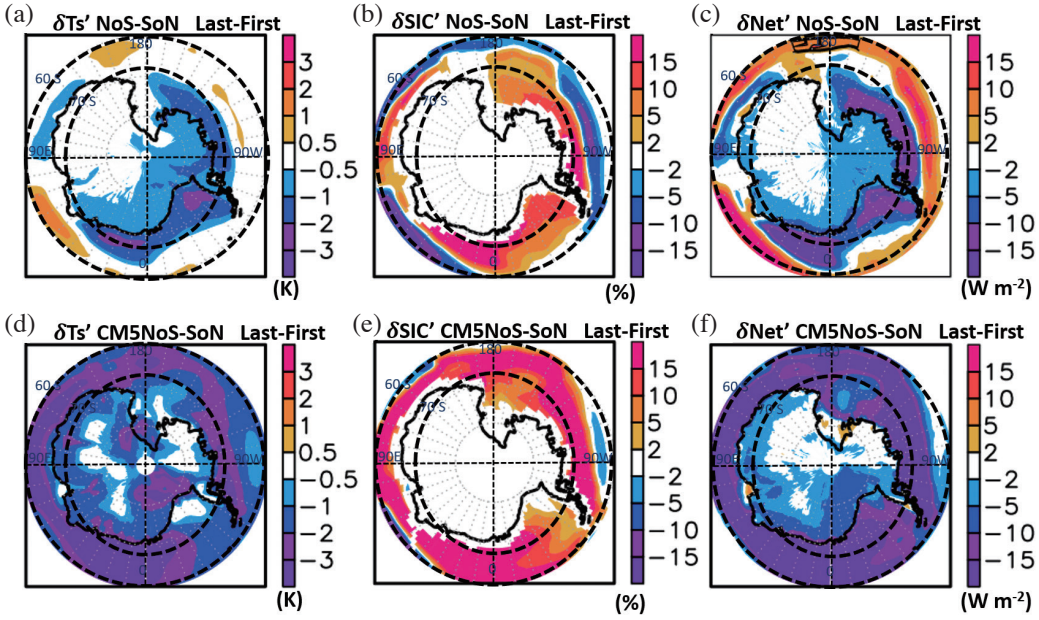

Fig. 10. The annual mean changes between the last 20 years and first 20 years in 1pctCO2 scenario (i.e., the last 20 years minus the first 20 years) from NoS minus SoN for (a) surface skin temperature, δTs'; (b) sea ice concentration, δSIC'; and (c) surface net flux, δNet'. (d) - (f) Same as (a) - (c) but for CMIP5 multi-model mean (CM5-NoS).

between modelled and observed Antarctic sea-ice concentration and plays an indispensable role for present day simulations (Michibata et al. 2019; Stephens et al. 2020).

Given the fidelity and robust results with inclusion of FIREs in reducing model-observation discrepancy in sea ice extent reported in Li et al. (2017), we extended our experiment by excluding FIRE to project the future state of Antarctic sea ice under the 1pctCO2 scenario to investigate the impacts from FIREs according to the CMIP5 1pctCO2 scenario protocol. Figures 5 and 6 show the significant levels ($p < 0.05$) for the changes in 140-year averaged radiation fields, Ts and SIC and THK for DJF (Fig. 5) and JJA (Fig. 6). The stippled areas indicating the impacts on the difference between two simulations with the inclusion (CESM1-SoN) and exclusion (CESM1-NoS) of FIREs are all significant for radiation fields, skin temperature and sea ice changes, showing the robust differences between the two simulations.

For the CMIP5 models without FIREs and CESM1-NoS, the total cloud ice-water path that influences radiation calculation is less by 70 - 80% relative to CESM1-SoN over much of the Southern Ocean in the initial warming period (figure not shown). This difference contributes to reduced downward longwave radiation and increased downward surface shortwave radiation during the 140 years runs. This net downward radiation reduction changes sea-ice area over Southern Oceans in the CESM1-NoS minus CESM1-SoN and CMIP5-NoS minus CESM1-SoN. The geographical pattern of SIC and radiation field changes in CESM1-NoS minus CESM1-SoN with progressive global warming largely matches the CMIP5-NoS minus CESM1-SoN.

In winter season (JJA), it appears that the changes resulting from FIREs contribution and the response under increasing CO_2 in sea ice are driven by an increase in downward longwave radiation due to increased cloud ice and water path with the inclusion of falling ice. The increased warming restricts the growth of sea ice, leading to a faster melting rate in sea-ice concentration, area and thickness for the long-term trend during the 140-year integration, which contributes to a reduced amplitude of the annual cycle of sea ice variation. On the other hand, during summer (DJF), the situation is more complex involving offsets between RLDS, RSDS, and RSUS, i.e., when FIREs are excluded, more sea ice increases albedo, leading to increased downward SW. It is due to the surface reflected SW (larger albedo) sufficiently large so that the net radiative flux decrease, resulting in increased sea-ice concentration and thickness. With inclusion of FIRE, net flux warming change restricts sea-ice growth, thinning sea ice thickness and thus reduces surface albedo in austral summer. This effect then offsets the reduced amount of solar radiation reaching to the surface. These findings are largely consistent with Li et al. (2020) regarding the roles of FIREs on sea ice projection of the Arctic, but surface temperature change is much more important for the Arctic sea ice than for the Southern Ocean sea ice due to the fact that the Arctic sea ice is surrounded by lands.

In terms of long-term trends, we found that the annual mean changes of sea ice thickness from first 20-year to mid 20-year are small (Fig. A6a), while it is thicker in CESM1-NoS relative to CESM1-SoN or becomes more thinning in CESM1-SoN over the location of SIC decreasing after mid 20-year to last 20-year (Fig. A6b). It is found that at the end of the 140-year simulation, the area-average SIC is 8%, 8%, and 5%, for CMIP5-MMM, CESM1-NoS, and CESM1-SoN, respectively. The area average of SIC at 8% at 100 model year run relative to CESM1-SoN as a reference, it would take another 40 years for both CESM1-NoS and CMIP5-MMM to reach 5% SIC relative to CESM1-SoN at year 140. For CMIP5-NoS MMM the SIC never reaches sea ice free at year 140 in any season, while sea ice free is simulated at year 130 for CESM1-NoS and at year 110 for CESM1-SoN in the peak melting season (February to March). Note that compared to Arctic oceans, sea ice free is simulated earlier for the Arctic, at year 100 for CESM1-NoS and year 70 for CESM1-SoN (Li et al. 2020).

The steadily increasing atmospheric CO_2 concentration leading to the spatial pattern of change in radiative properties, SIC, sea ice thickness and Ts across the Southern Ocean is typically weaker in CESM1-NoS relative to CESM1-SoN. That is to say, local changes in radiative fluxes, Ts, SIC, and thickness are enhanced in a more robust manner with inclusion of FIRE. The mass changes have fewer impacts on sea ice changes from surface snowfall rate, indicating the energy adjustment rather than mass balance on the sea ice simulations. The sea ice thickness seasonal changes in DJF and in JJA between the last 20-year and first 20-year are similar to the SIC changes, showing more melting of SIC and more thinning of THK in DJF than in JJA.

Patterns of change are somewhat similar between CMIP5 models without FIRE and CESM1-NoS. This resemblance potentially implies that an improper representation of the FIREs contributes, at least partially, to differences in the simulation of Southern Ocean climate change under CO_2-driven warming.

We acknowledge the extensive studies from many recent studies (e.g., Martin et al. 2013; Zunz et al. 2013; Kay et al. 2015; Rosenblum and Eisenman 2017; Singh et al. 2019; Zhang et al. 2019; Lehner et al. 2020) regarding the potential contribution from internal climate variability. Internal variability could be one of the factors that influence the potential impact of the FIREs on sea ice change projection presented in this study. We did consider to use the large ensemble data available from the CESM-LE project (Kay et al. 2015) to investigate if the impacts of NoS and SoN changes are larger than the internal variability under climate changes, but our study focuses on climate

changes under 1pctCO2 while the output from CESM-LE is for RCP8.5 scenario. A newer CESM1 version was used in the CESM-LE project. It is not affordable to run a large ensemble with NoS using fully-coupled CESM1-CAM5, following the protocol of CMIP5. Alternatively, we take advantage of the results presented in Singh et al. (2019), who investigated the internal variability over Southern Oceans and used the 40-members of CESM-LE. The differences in sea ice area and skin temperature between CESM1-NoS and CESM1-SoN simulations presented in this study are much larger than the standard deviation reported from Singh et al. (2019). The standard deviation of the annual mean sea ice area from CESM-LE is approximately 0.5 million km^2 [see Fig. 1a in Singh et al. (2019)]. The sea ice area of NoS-SoN difference in this study is above one standard deviation of 0.5 million km^2 during the entire 140 years (except the first several years) and above 2 - 3 standard deviations after 40 model years (not shown). While we found the significant impacts from the FIREs on the changes of sea ice, skin temperature and radiation budgets, we acknowledge that there are caveats and limitations for not considering the internal variability's contributions to the sea ice changes due to using a single model simulation in this study (Lehner et al. 2020). We do not argue, however, that FIRE is the only dominant process in model response to the climate changes related to sea ice change. The results presented in this study have shown that FIREs are an important process for simulating the climate changes of radiative balance and sea-ice concentration over the Southern Ocean under progressive global warming. Our results suggest that FIRE is potentially an important process with substantial effects on simulated energy budgets and sea ice. Such a physics-based improvement, if applied across all models, would increase our confidence and narrow the model spread on the projections of regional changes affecting climate feedbacks.

Acknowledgements The contribution by JLL to this study was carried out on behalf of the Jet Propulsion Laboratory, California Institute of Technology with the National Aeronautics and Space Administration (NASA).

REFERENCES

Aagaard, K., 1989: A synthesis of the Arctic Ocean circulation. *Rapp. P.-V. Réun. Cons. Int. Explor. Mer*, **188**, 11-22.

Aagaard, K. and E. C. Carmack, 1989: The role of sea ice and other fresh water in the Arctic circulation. *J. Geophys. Res.*, **94**, 14485-14498, doi: 10.1029/jc094ic10p14485. [Link]

Armour, K. C., C. M. Bitz, and G. H. Roe, 2013: Time-varying climate sensitivity from regional feedbacks. *J. Clim.*, **26**, 4518-4534, doi: 10.1175/JCLI-D-12-00544.1. [Link]

Armour, K. C., J. Marshall, J. R. Scott, A. Donohoe, and E. R. Newsom, 2016: Southern Ocean warming delayed by circumpolar upwelling and equatorward transport. *Nat. Geosci.*, **9**, 549-554, doi: 10.1038/ngeo2731. [Link]

Beszczynska-Möller, A., R. A. Woodgate, C. Lee, H. Melling, and M. Karcher, 2011: A synthesis of exchanges through the main oceanic gateways to the Arctic Ocean. *Oceanography*, **24**, 82-99, doi: 10.5670/oceanog.2011.59. [Link]

Bintanja, R. and F. M. Selten, 2014: Future increases in Arctic precipitation linked to local evaporation and sea-ice retreat. *Nature*, **509**, 479-482, doi: 10.1038/nature13259. [Link]

Bracegirdle, T. J., W. M. Connolley, and J. Turner, 2008: Antarctic climate change over the twenty first century. *J. Geophys. Res.*, **113**, doi: 10.1029/2007jd008933. [Link]

Bracegirdle, T. J., D. B. Stephenson, J. Turner, and T. Phillips, 2015: The importance of sea ice area biases in 21st century multimodel projections of Antarctic temperature and precipitation. *Geophys. Res. Lett.*, **42**, 10832-10839, doi: 10.1002/2015GL067055. [Link]

Cesana, G., J. E. Kay, H. Chepfer, J. M. English, and G. Boer, 2012: Ubiquitous low-level liquid-containing Arctic clouds: New observations and climate model constraints from CALIPSO-GOCCP. *Geophys. Res. Lett.*, **39**, L20804, doi: 10.1029/2012GL053385. [Link]

Comiso, J. C., 2009: Variability and trends of the global sea ice cover. In: Thomas, D. N. and G. S. Dieckmann (Eds.), Sea Ice, Second Edition, Wiley, Blackwell, Oxford, 205-246, doi: 10.1002/9781444317145.ch6. [Link]

Comiso, J. C., R. Kwok, S. Martin, and A. L. Gordon, 2011: Variability and trends in sea ice extent and ice production in the Ross Sea. *J. Geophys. Res.*, **116**, doi: 10.1029/2010JC006391. [Link]

Gettelman, A., X. Liu, S. J. Ghan, H. Morrison, S. Park, A. J. Conley, S. A. Klein, J. Boyle, D. L. Mitchell, and J.-L. F. Li, 2010: Global simulations of ice nucleation and ice supersaturation with an improved cloud scheme in the Community Atmosphere Model. *J. Geophys. Res.*, **115**, D18216, doi: 10.1029/2009JD013797. [Link]

Hosking, J. S., A. Orr, T. J. Bracegirdle, and J. Turner, 2016: Future circulation changes off West Antarctica: Sensitivity of the Amundsen Sea Low to projected anthropogenic forcing. *Geophys. Res. Lett.*, **43**, 367-376, doi: 10.1002/2015gl067143. [Link]

IPCC, 2013: Climate Change 2013: The Physical Science Basis, Contribution of Working Group I to the Fifth Assessment Report of the Intergovernmental Panel on Climate Change, Cambridge University Press, Cambridge,

United Kingdom and New York, NY, USA, 1535 pp.

Kay, J. E., C. Deser, A. Phillips, A. Mai, C. Hannay, G. Strand, J. M. Arblaster, S. C. Bates, G. Danabasoglu, J. Edwards, M. Holland, P. Kushner, J.-F. Lamarque, D. Lawrence, K. Lindsay, A. Middleton, E. Munoz, R. Neale, K. Oleson, L. Polvani, and M. Vertenstein, 2015: The Community Earth System Model (CESM) Large Ensemble project: A community resource for studying climate change in the presence of internal climate variability. *Bull. Amer. Meteorol. Soc.*, **96**, 1333-1349, doi: 10.1175/bams-d-13-00255.1. [Link]

Kay, J. E., L. Bourdages, N. B. Miller, A. Morrison, V. Yettella, H. Chepfer, and B. Eaton, 2016a: Evaluating and improving cloud phase in the Community Atmosphere Model version 5 using spaceborne lidar observations. *J. Geophys. Res.*, **121**, 4162-4176, doi: 10.1002/2015JD024699. [Link]

Kay, J. E., C. Wall, V. Yettella, B. Medeiros, C. Hannay, P. Caldwell, and C. Bitz, 2016b: Global climate impacts of fixing the Southern Ocean shortwave radiation bias in the Community Earth System Model (CESM). *J. Clim.*, **29**, 4617-4636, doi: 10.1175/JCLI-D-15-0358.1. [Link]

Lee, W.-L., J.-L. F. Li, K.-M. Xu, E. Suhas, J. H. Jiang, Y.-H. Wang, G. Stephens, E. Fetzer, and J.-Y. Yu, 2019: Relating precipitating ice radiative effects to surface energy balance and temperature biases over the Tibetan Plateau in winter. *J. Geophys. Res.*, **124**, 12455-12467, doi: 10.1029/2018JD030204. [Link]

Lefebvre, W. and H. Goosse, 2007: Analysis of the projected regional sea-ice changes in the Southern Ocean during the twenty-first century. *Clim. Dyn.*, **30**, 59-76, doi: 10.1007/s00382-007-0273-6. [Link]

Lehner, F., C. Deser, N. Maher, J. Marotzke, E. M. Fischer, L. Brunner, R. Knutti, and E. Hawkins, 2020: Partitioning climate projection uncertainty with multiple large ensembles and CMIP5/6. *Earth Syst. Dynam.*, **11**, 491-508, doi: 10.5194/esd-11-491-2020. [Link]

Li, J.-L. F., M. Richardson, Y. Hong, W.-L. Lee, Y.-H. Wang, J.-Y. Yu, E. Fetzer, G. Stephens, and Y. Liu, 2017: Improved simulation of Antarctic sea ice due to the radiative effects of falling snow. *Environ. Res. Lett.*, **12**, 084010, doi: 10.1088/1748-9326/aa7a17. [Link]

Li, J.-L. F., W.-L. Lee, K.-M. Xu, J. Jiang, E. Fetzer, C.-A. Chen, Y.-H. Wang, J.-Y. Yu, P.-C. Hsu, and H.-H. Hsu, 2020: The role of falling ice radiative effects on climate projections over Arctic under global warming. *Terr. Atmos. Ocean. Sci.*, **31**, 633-648, doi: 10.3319/TAO.2020.04.29.01. [Link]

Mahlstein, I., P. R. Gent, and S. Solomon, 2013: Historical Antarctic mean sea ice area, sea ice trends, and winds in CMIP5 simulations. *J. Geophys. Res.*, **118**, 5105-5110, doi: 10.1002/jgrd.50443. [Link]

Maksym, T., S. E. Stammerjohn, S. Ackley, and R. Massom, 2012: Antarctic sea ice—A polar opposite? *Oceanography*, **25**, 140-151, doi: 10.5670/oceanog.2012.88. [Link]

Martin, T., W. Park, and M. Latif, 2013: Multi-centennial variability controlled by Southern Ocean convection in the Kiel Climate Model. *Clim. Dyn.*, **40**, 2005-2022, doi: 10.1007/s00382-012-1586-7. [Link]

McCoy, D. T., D. L. Hartmann, M. D. Zelinka, P. Ceppi, and D. P. Grosvenor, 2015: Mixed-phase cloud physics and Southern Ocean cloud feedback in climate models. *J. Geophys. Res.*, **120**, 9539-9554, doi: 10.1002/2015jd023603. [Link]

Medley, B., J. R. McConnell, T. A. Neumann, C. H. Reijmer, N. Chellman, M. Sigl, and S. Kipfstuhl, 2018: Temperature and snowfall in western Queen Maud Land increasing faster than climate model projections. *Geophys. Res. Lett.*, **45**, 1472-1480, doi: 10.1002/2017GL075992. [Link]

Meijers, A. J. S., 2014: The Southern Ocean in the coupled model intercomparison project phase 5. *Phil. Trans. Math. Phys. Eng. Sci.*, **372**, 20130296, doi: 10.1098/rsta.2013.0296. [Link]

Meijers, A. J. S., E. Shuckburgh, N. Bruneau, J.-B. Sallee, T. J. Bracegirdle, and Z. Wang, 2012: Representation of the Antarctic Circumpolar Current in the CMIP5 climate models and future changes under warming scenarios. *J. Geophys. Res.*, **117**, C12008, doi: 10.1029/2012JC008412. [Link]

Michibata, T., K. Suzuki, M. Sekiguchi, and T. Takemura, 2019: Prognostic Precipitation in the MIROC6-SPRINTARS GCM: Description and Evaluation Against Satellite Observations. *J. Adv. Model. Earth Syst.*, **11**, 839-860, doi: 10.1029/2018MS001596. [Link]

Morrison, H. and A. Gettelman, 2008: A new two-moment bulk stratiform cloud microphysics scheme in the Community Atmosphere Model, Version 3 (CAM3). Part I: Description and numerical tests. *J. Clim.*, **21**, 3642-3659, doi: 10.1175/2008jcli2105.1. [Link]

Neale, R. B., C.-C. Chen, A. Gettelman, P. H. Lauritzen, S. Park, D. L. Williamson, A. J. Conley, R. Garcia, D. Kinnison, J.-F. Lamarque, D. Marsh, M. Mills, A. K. Smith, S. Tilmes, F. Vitt, H. Morrison, P. Cameron-Smith, W. D. Collins, M. J. Iacono, R. C. Easter, S. J. Ghan, X. Liu, P. J. Rasch, and M. A. Taylor, 2012: Description of the NCAR Community Atmosphere Model (CAM 5.0). NCAR Technical Note, NCAR/TN-486+STR, National Center for Atmospheric Research, Boulder, Colorado, USA, 274 pp.

Nghiem, S. V., I. G. Rigor, P. Clemente-Colón, G. Neumann, and P. P. Li, 2016: Geophysical constraints on

the Antarctic sea ice cover. *Remote Sens. Environ.*, **181**, 281-292, doi: 10.1016/j.rse.2016.04.005. [Link]

Palerme, C., C. Genthon, C. Claud, J. E. Kay, N. B. Wood, and T. L'Ecuyer, 2017: Evaluation of current and projected Antarctic precipitation in CMIP5 models. *Clim. Dyn.*, **48**, 225-239, doi: 10.1007/s00382-016-3071-1. [Link]

Parkinson, C. L., 2019: A 40-y record reveals gradual Antarctic sea ice increases followed by decreases at rates far exceeding the rates seen in the Arctic. *Proc. Natl. Acad. Sci.*, **116**, 14414-14423, doi: 10.1073/pnas.1906556116. [Link]

Polvani, L. M. and K. L. Smith, 2013: Can natural variability explain observed Antarctic sea ice trends? new modeling evidence from CMIP5. *Geophys. Res. Lett.*, **40**, 3195-3199, doi: 10.1002/grl.50578. [Link]

Raphael, M. N., G. J. Marshall, J. Turner, R. L. Fogt, D. Schneider, D. A. Dixon, J. S. Hosking, J. M. Jones, and W. R. Hobbs, 2016: The Amundsen sea low: Variability, change, and impact on Antarctic climate. *Bull. Amer. Meteorol. Soc.*, **97**, 111-121, doi: 10.1175/bams-d-14-00018.1. [Link]

Rosenblum, E. and I. Eisenman, 2017: Sea ice trends in climate models only accurate in runs with biased global warming. *J. Clim.*, **30**, 6265-6278, doi: 10.1175/jcli-d-16-0455.1. [Link]

Scott, M., 2019: Understanding climate: Antarctic sea ice extent. Available at https://www.climate.gov/news-features/understanding-climate/understanding-climate-antarctic-sea-ice-extent (last access, 21 April 21 2020).

Simmonds, I., 2015: Comparing and contrasting the behaviour of Arctic and Antarctic sea ice over the 35 year period 1979-2013. *Ann. Glaciol.*, **56**, 18-28, doi: 10.3189/2015AoG69A909. [Link]

Singh, H. A., L. M. Polvani, and P. J. Rasch, 2019: Antarctic sea ice expansion, driven by internal variability, in the presence of increasing atmospheric CO_2. *Geophys. Res. Lett.*, **46**, 14762-14771, doi: 10.1029/2019GL083758. [Link]

Smith, W. O., M. S. Dinniman, E. E. Hofmann, and J. M. Klinck, 2014: The effects of changing winds and temperatures on the oceanography of the Ross Sea in the 21st century. *Geophys. Res. Lett.*, **41**, 1624-1631, doi: 10.1002/2014gl059311. [Link]

Stammerjohn, S. E., D. G. Martinson, R. C. Smith, X. Yuan, and D. Rind, 2008: Trends in Antarctic annual sea ice retreat and advance and their relation to El Niño–Southern Oscillation and Southern Annular Mode variability. *J. Geophys. Res.*, **113**, C03S90, doi: 10.1029/2007JC004269. [Link]

Stephens, G. L., J. M. Slingo, E. Rignot, J. T. Reager, M. Z. Hakuba, P. J. Durack, J. Worden, and R. Rocca, 2020: Earth's water reservoirs in a changing climate. *Proc. R. Soc. London Ser. A-Math. Phys. Eng. Sci.*, **476**, 20190458, doi: 10.1098/rspa.2019.0458. [Link]

Taylor, K. E., R. J. Stouffer, and G. A. Meehl, 2012: An Overview of CMIP5 and the Experiment Design. *Bull. Amer. Meteorol. Soc.*, **93**, 485-498, doi: 10.1175/bams-d-11-00094.1. [Link]

Trenberth, K. E. and J. T. Fasullo, 2010: Simulation of Present-Day and Twenty-First-Century Energy Budgets of the Southern Oceans. *J. Clim.*, **23**, 440-454, doi: 10.1175/2009jcli3152.1. [Link]

Turner, J. and J. Overland, 2009: Contrasting climate change in the two polar regions. *Polar Res.*, **28**, 146-164, doi: 10.1111/j.1751-8369.2009.00128.x. [Link]

Turner, J., T. J. Bracegirdle, T. Phillips, G. J. Marshall, and J. S. Hosking, 2013: An Initial Assessment of Antarctic Sea Ice Extent in the CMIP5 Models. *J. Clim.*, **26**, 1473-1484, doi: 10.1175/jcli-d-12-00068.1. [Link]

Turner, J., J. S. Hosking, T. J. Bracegirdle, G. J. Marshall, and T. Phillips, 2015: Recent changes in Antarctic sea ice. *Philos. Trans. R. Soc. A-Math. Phys. Eng. Sci.*, **373**, 20140163, doi: 10.1098/rsta.2014.0163. [Link]

Van den Broeke, M. R., 2004: On the role of Antarctica as heat sink for the global atmosphere. *J. Phys. IV*, **121**, 115-124, doi: 10.1051/jp4:2004121006. [Link]

Zhang, L., T. L. Delworth, W. Cooke, and X. Yang, 2019: Natural variability of Southern Ocean convection as a driver of observed climate trends. *Nat. Clim. Change*, **9**, 59-65, doi: 10.1038/s41558-018-0350-3. [Link]

Zunz, V., H. Goosse, and F. Massonnet, 2013: How Does Internal Variability Influence the Ability of CMIP5 Models to Reproduce the Recent Trend in Southern Ocean Sea Ice Extent? *The Cryosphere*, **7**, 451-468, doi: 10.5194/tc-7-451-2013. [Link]

APPENDIX

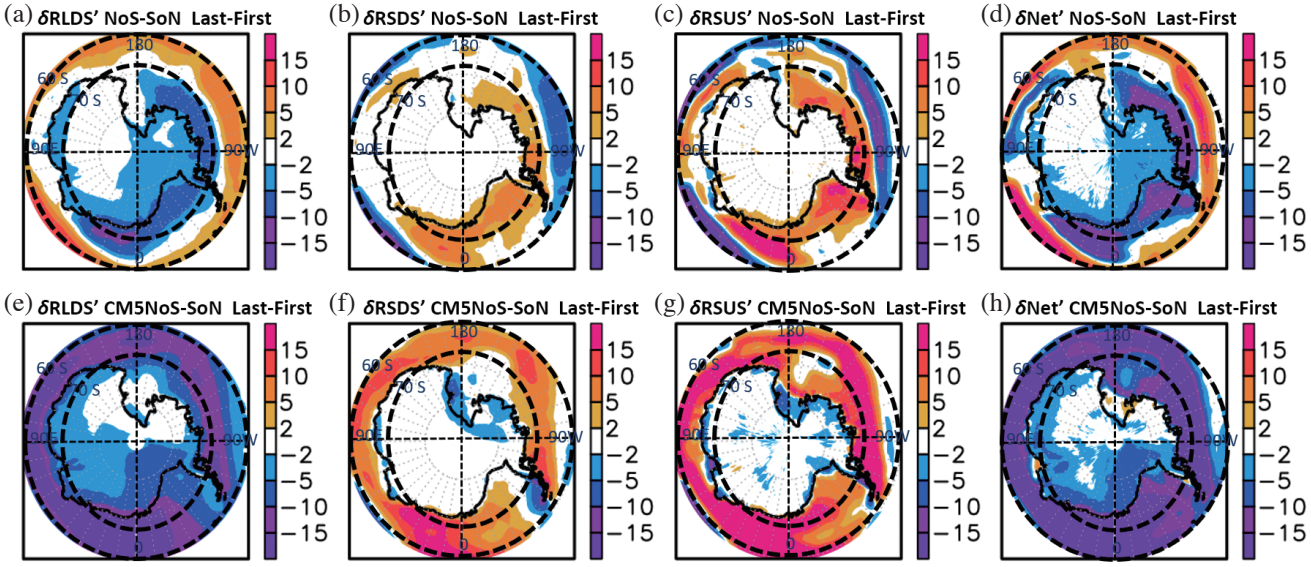

Fig. A1. As in Fig. 7, but for the changes between annual mean of the last 20 years and first 20 years in 1pctCO2 scenario (i.e., the last 20 years minus the first 20 years) from NoS minus SoN for (a) surface downward longwave radiation, δRLDS'; (b) surface downward shortwave radiation, δRSDS'; (c) surface upward shortwave radiation, δRSUS'; and (d) surface net flux, δNet'. (e) - (h) Same as (a) - (d) but for CMIP5 multi-model mean (CMIP5-NoS).

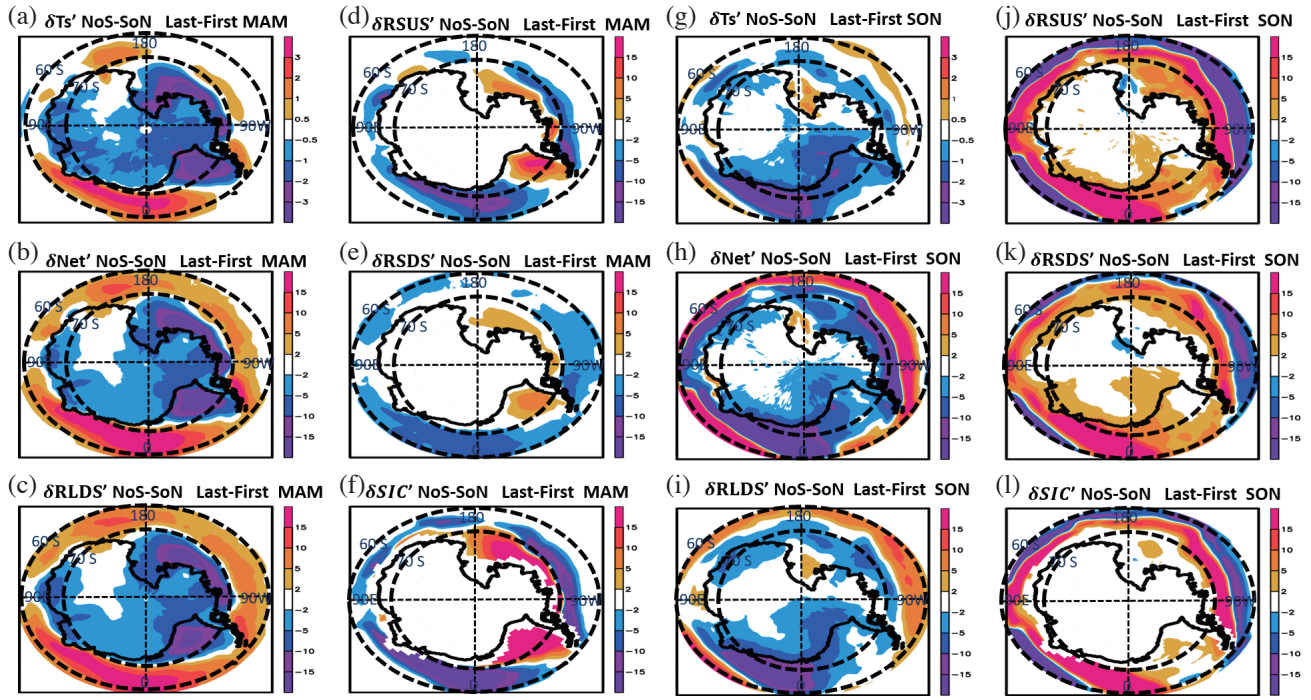

Fig. A2. As in Fig. 8, but for the changes between last 20 years and first 20 years in 1pctCO2 scenario (i.e., the last 20 years minus the first 20 years) for March-April-May (MAM) from SoN minus SoN for (a) surface skin temperature, δTs'; (b) surface ice concentration, δSIC'; (c) net flux, δNet'; (d) surface downward longwave radiation, δRLDS'; (e) surface upward shortwave radiation, δRSUS'; and (f) surface downward shortwave radiation, δRSDS', from NoS-SoN. (g) - (l) Same as (a) - (f) but for September-October-November (SON).

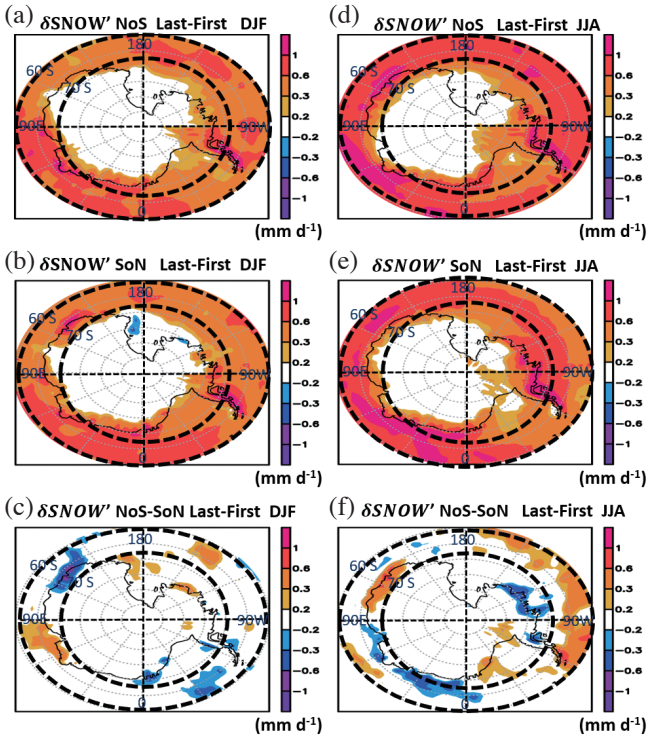

Fig. A3. The changes of surface snow fall rate (mm d^{-1}) between last 20 years and first 20 years in 1pctCO2 scenario (i.e., the last 20 years minus the first 20 years) for DJF in case of (a) NoS, (b) SoN, and (c) NoS-SoN. (d) - (f) Same as in (a) - (c) but for June-July-August (JJA).

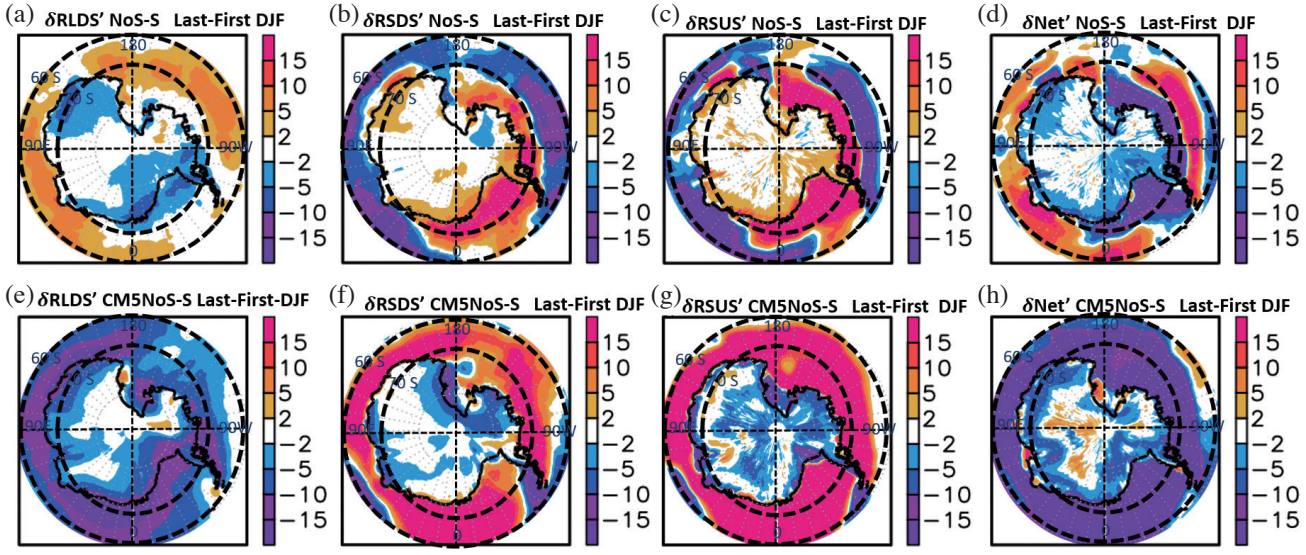

Fig. A4. As in Fig. 7, but for June-July-August (JJA) and for the changes between the last 20 years and first 20 years in 1pctCO2 scenario (i.e., the last 20 years minus the first 20 years) from NoS minus SoN for (a) surface downward longwave radiation, δRLDS'; (b) surface downward shortwave radiation, δRSDS'; (c) surface upward shortwave radiation, δRSUS'; and (d) surface net flux, δNet'. (e) - (h) Same as (a) - (d) but for CMIP5 multi-model mean (CM5-NoS).

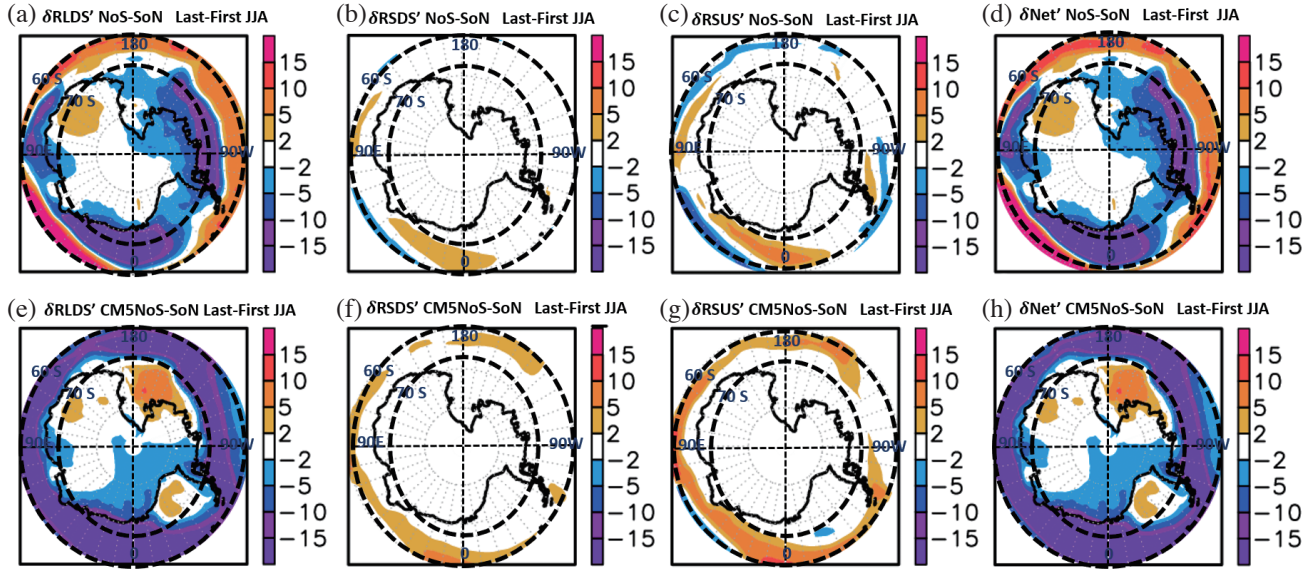

Fig. A5. As in Fig. A3, but for December-January-February (DJF) for the changes between mean of the last 20 years and first 20 years in 1pctCO2 scenario (i.e., the last 20 years minus the first 20 years) from NoS minus SoN for (a) surface downward longwave radiation, δRLDS'; (b) surface downward shortwave radiation, δRSDS'; (c) surface upward shortwave radiation, δRSUS'; and (d) surface net flux, δNet'. (e) - (h) Same as (a) - (d) but for CMIP5 multi-model mean (CM5-NoS).

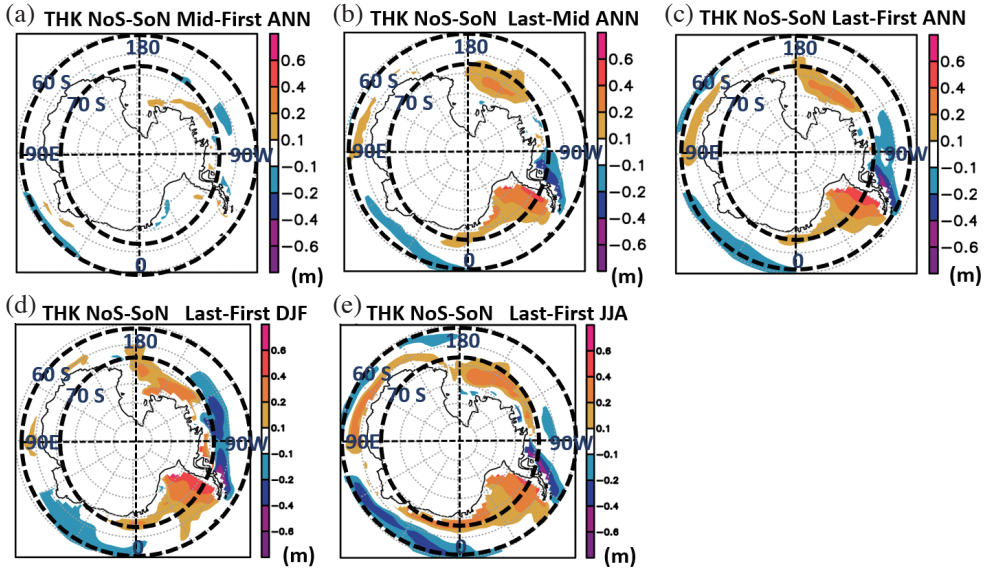

Fig. A6. (a) The difference of sea ice thickness (THK) between Snow-Radiative off minus Snow-radiative on (NoS-SoN) annual mean from the first 20 years (1 - 20 years: First) and middle 20 years (60 - 80 years: Mid); same as (a) but for the difference between Mid and last 20 years (120 - 140 years: Last). (c) Same as (b) but for Last minus First 20 years. (d) same as (c) but for DJF. (e) Same as (d) but for JJA. The SoN and SoN are CESM1 experiments integrated for 140 years, following the CMIP5 1pctCO2 scenario.